ACS Photonics

Article

pubs.acs.org/journal/apchd5

Size Tunable ZnO Nanoparticles To Enhance Electron Injection in Solution Processed QLEDs

Jiangyong Pan,[†,‡] Jing Chen,[†,‡] Qianqian Huang,[†] Qasim Khan,[†] Xiang Liu,[†] Zhi Tao,[†] Zichen Zhang,[§] Wei Lei,[*,†] and Arokia Nathan[*,†,∥]

[†]School of Electronic Science and Engineering, Southeast University, Nanjing 210096, China

[§]State Key Laboratory of Precision Measurement Technology and Instruments, Department of Precision Instrument, Tsinghua University, Beijing 100084, China

[∥]Electrical Engineering Division, Engineering Department, University of Cambridge, 9 JJ Thomson Avenue, CB3 0FA, Cambridge, United Kingdom

Supporting Information

ABSTRACT: Quantum dot (QD) light-emitting diodes (LEDs) are a promising candidate for high-efficiency, color-saturated displays. This work reports on the size effect of sol−gel synthesized ZnO nanoparticles (NPs) in which sizes of 2.9, 4.0, and 5.5 nm, were used as an electron transfer layer in QLEDs. The size of the NPs was estimated by transmission electron microscopy (TEM) and its effect on QLED performance was investigated by photoluminescence decay lifetime and electron mobility of ZnO NPs. It was found that as the size of the NP decreased from 5.5 to 2.9 nm, the conductivity increased, whereby the electron mobility was enhanced from 7.2×10^{-4} $cm^2/V{\cdot}s$ to 4.8×10^{-3} $cm^2/V{\cdot}s$ and electron decay lifetime increased from 5.11 to 6.68 ns. A comparison of NP size effects shows that the best performance is achieved with the 2.9 nm sized ZnO, which yields a turn on voltage of 3.3 V, a maximum current efficiency of 12.5 cd/A, power efficiency of 4.69 lm/W and external quantum efficiencies (EQE) of 4.2%. This is most likely due to the higher electron mobility in the smaller ZnO NPs, which facilitates electron transfer from the NPs to QDs, along with the slow exciton dissociation in the QD layer as a result of more favorable energy level alignment at the interface of smaller ZnO NPs and the adjacent emissive layer.

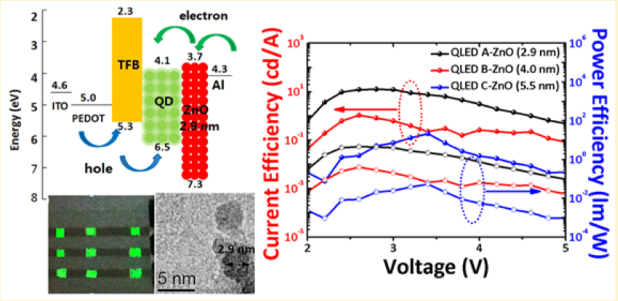

KEYWORDS: *quantum dot, light-emitting diode, ZnO NPs, size dependency, band gap*

Semiconductor nanocrystals or quantum dots (QDs) have been widely employed in light emitting diodes (LEDs) because the QDs exhibit a variety of desirable features including size-tunable photoluminescence (PL), narrow emission line width, high PL quantum yield, superior photostability, and flexible solution processability.[1,2] Since the earliest report on quantum LEDs (QLEDs) in 1994, many approaches have been studied to improve the performance of QLEDs, including the preparation of novel materials, optimization of the balance of carrier injection, and design of novel device structures.[3] In earlier works, thick QD layers were used, which were acting as both emissive and electron transport layers (ETL) leading to low luminous efficiencies. Later, the efficiencies were vastly improved by virtue of a physical separation between the QD emissive layer and the electron transport layer (ETL). This facilitates efficient electron transport to the QD layer as well as provide confinement of excitons.[2] In addition, much effort has been made to substitute the organic for inorganic material as the charge transport layer in QLEDs so as to overcome the persistent drawbacks, such as moisture/oxygen-induced degradation and the thermal instability,[4] associated with the former. Thus, QLEDs featuring inorganic layers are promising from the standpoint of long lifetime without stringent encapsulation requirements.

A variety of metal-oxide materials as electron transport layers in QLEDs have been demonstrated, in an attempt to realize an all-solution-processed QLED.[5] For example, amorphous TiO_2 prepared by a sol−gel method has been widely utilized in numerous devices as a charge transport layer.[6] However, its carrier mobility is limited in the amorphous phase as compared to the crystalline counterpart. The electron mobility of solution based TiO_2 is about 1×10^{-4} $cm^2/V{\cdot}s$, which is 4 orders of magnitude lower than that of the crystalline counterpart (~1 $cm^2/V{\cdot}s$).[7] More recently ZnO nanoparticles (NPs) have emerged as a suitable alternative. In comparison to organics, the oxides have higher thermal stability and reduced sensitivity to oxygen and moisture.[8] In particular, the higher electron mobility of ZnO (2×10^{-3} $cm^2/V{\cdot}s$) facilitates efficient electron transport, thereby increasing the efficiency of charge

Received: May 17, 2015
Published: January 22, 2016

DOI: 10.1021/acsphotonics.5b00267
ACS Photonics 2016, 3, 215−222

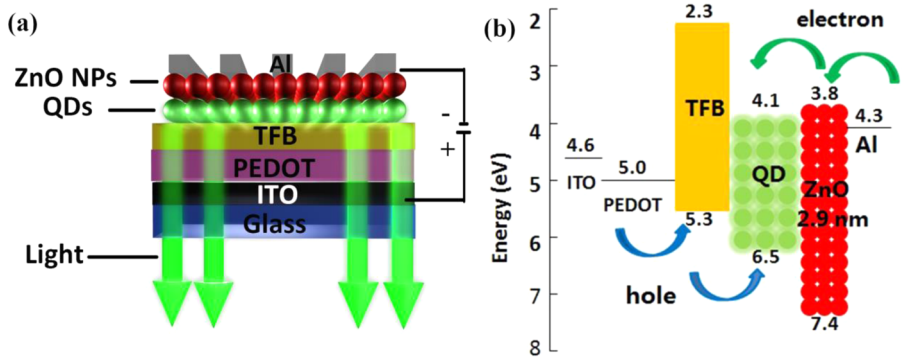

Figure 1. (a) Structure and (b) energy level diagram for the various layers of QLEDs.

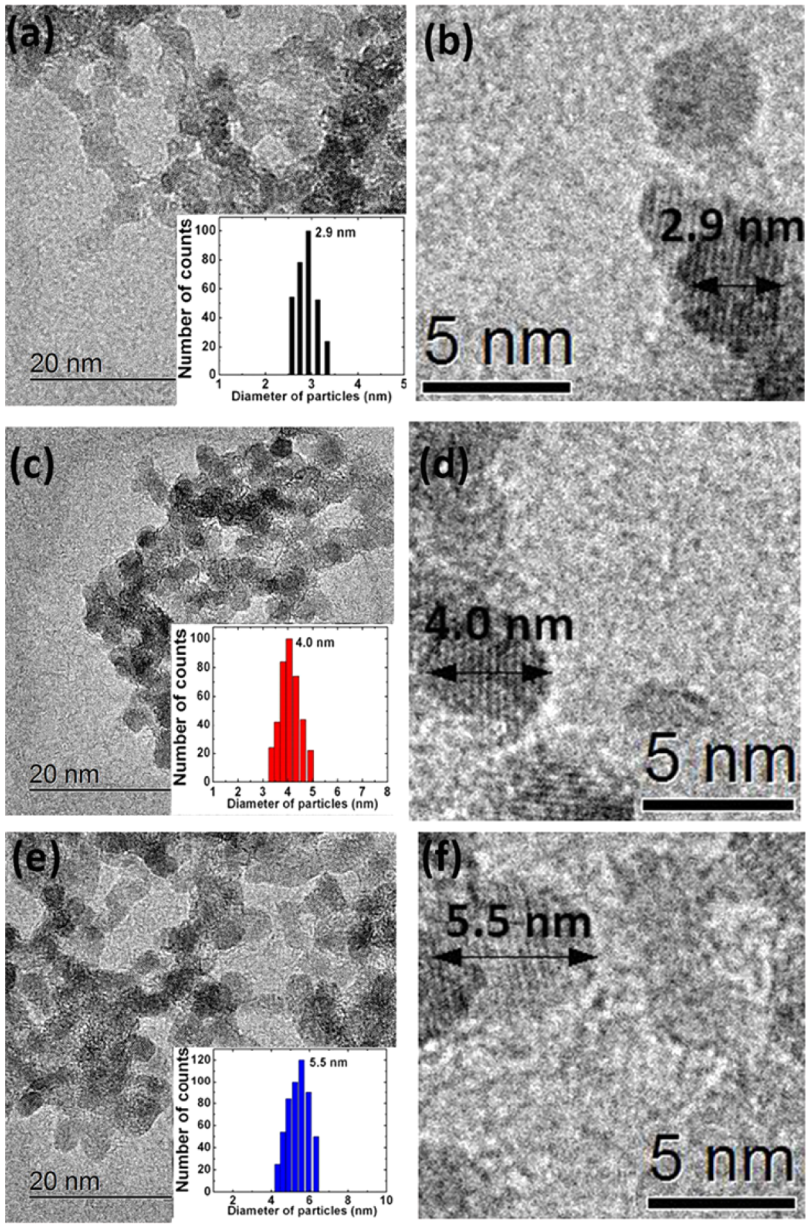

Figure 2. TEM and HRTEM images of the three sizes of ZnO NPs. Corresponding $[Zn^{2+}]/[OH^-]$ ratio is (a, b) 1:0.5, (c, d) 1:1, and (e, f) 1:1.5. Inset shows the statistical distribution images of particle size.

recombination.[9] Moreover, the band offset in ZnO is favorable for electron transfer and equally conducive to hole confinement in the adjacent QD layer, thereby boosting the charge recombination efficiency of the QLED.[10] Thus, ZnO NPs can be considered as a suitable candidate for the ETL in the QLEDs.

DOI: 10.1021/acsphotonics.5b00267
ACS Photonics 2016, 3, 215−222

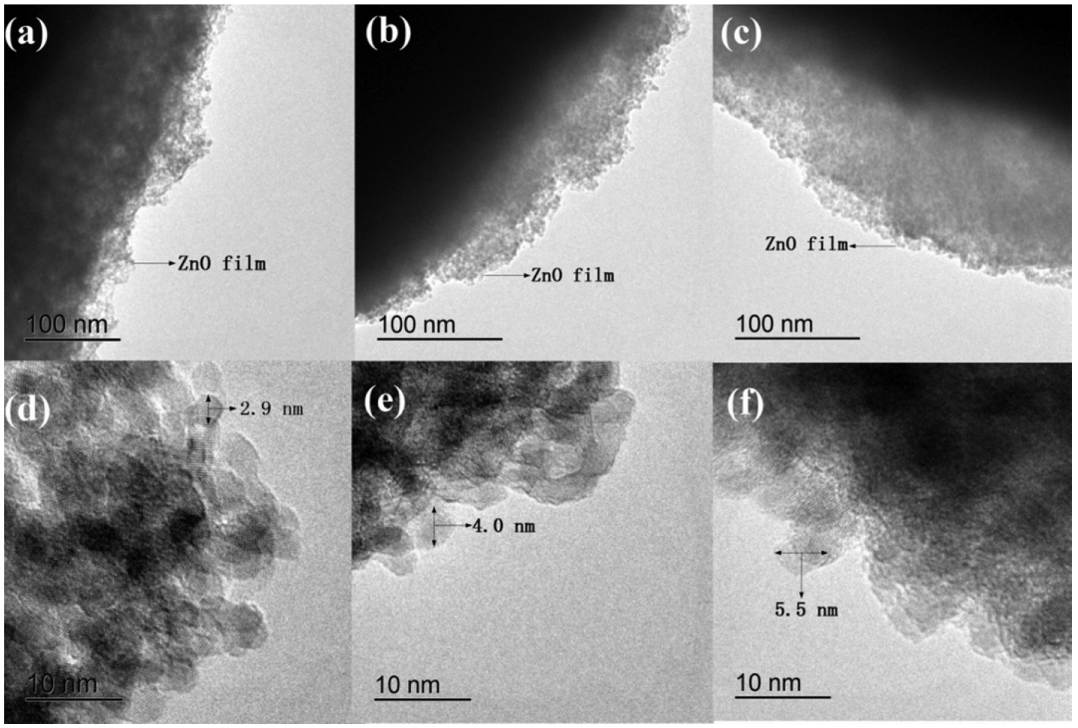

Figure 3. TEM and HRTEM images of ZnO film of the different sized ZnO NPs: (a, d) 2.9, (b, e) 4.0, and (c, f) 5.5 nm.

Despite the progress, a number of issues remain for ZnO-based QLEDs.[11] The challenges here are the low device efficiency in the brightness region of interest and the high turn-on voltage, all of which are strongly dependent on the transporting materials and device architectures. Thus, in this work, QLEDs based on ZnO NPs will be fabricated in an attempt to investigate the size dependency of the ZnO NPs on QLED performance.

EXPERIMENTAL SECTION

Chemicals. Cadmium oxide (CdO, 99.99%), zinc acetate (99.9%, powder), selenium (99.9%, powder), sulfur (99.9%, powder), trioctylphosphine (TOP, 90%), oleic acid (OA, 90%), 1-octadecene (ODE, 90%), zinc acetate (99.9%, powder), dimethyl sulfoxide (reagent grade, 99%), and tetramethylammonium hydroxide (99.99%, powder) were used as purchased from Aldrich.

Green emitting ZnCdSeS QDs were synthesized according to a modified method reported previously. Here, 0.4 mmol of CdO, 4 mmol of zinc acetate, 4 mmol of oleic acid (OA), and 20 mL of 1-octadecne were mixed in a 100 mL round flask. The mixture was heated to 150 °C degassed under ∼10 pa pressure for 30 min, filled with high-purity N_2 flowing, and further heated to 300 °C to form a clear solution of $Cd(OA)_2$ and $Zn(OA)_2$. At this temperature, a stock solution containing 3 mL of trioctylphosphine, 0.4 mmol of Se, and 4 mmol of S was quickly injected into the reaction flask. After the injection, the reaction temperature was maintained for 10 min to promote the growth of QDs. The reaction was subsequently cooled down to room temperature to stop further growth. The QDs were washed with acetone three times, and finally dispersed in toluene at a concentration of 10 mg/mL.

The ZnO NPs used in this study were synthesized through a sol−gel method. A solution of 0.1 M zinc acetate in dimethyl sulfoxide (DMSO) and 10 mL of 0.5 M tetramethylammonium hydroxide (TMAH) in ethanol were mixed and stirred for 1 h in ambient atmosphere.[9] The prepared product was collected by centrifugation and then washed twice with methanol. The transparent precipitate was redispersed in butanol to form a ZnO NPs solution with concentration 30 mg/mL. Three different sizes of ZnO samples were synthesized with the ratio of $[Zn^{2+}]/[OH^-]$ fixed at 1:0.5, 1:1, and 1:1.5 according to the method mentioned above.

The fabrication of QLEDs was completed in a nitrogen-filled glovebox, which normally has oxygen and moisture levels below 0.1 ppm located inside a class 10000 clean room. The fabrication process can be found in previously published work.[12] The thicknesses of PEDOT:PSS, TFB HTL, QD emitting layer, and ZnO NP ETL were 40, 20, 20, and 30 nm, respectively. The active area of the devices were defined by a shadow mask of 4 mm^2. The devices were named as samples A, B, and C with ZnO NP sizes of 2.9, 4.0, and 5.5 nm, respectively.

The films thicknesses were measured using Filmetrics F20-EXR, current−voltage (I−V) characteristics measured with a Keithley-2400 source-meter unit, and the absorption and photoluminescence (PL) spectra measured using the U-4100 UV−visible and NIR-300 spectrophotometer, respectively. The luminance was calibrated using a Minolta luminance meter (LS-100). Structural analysis of the samples was carried out using a Cs-corrected high-resolution transmission electron microscope (HRTEM, Tecnai G20).

RESULTS AND DISCUSSION

The structure and schematic energy band diagram of the QLED is shown in Figure 1a and b, respectively. Here, poly-(ethylenedioxythiophene):polystyrenesulfonate (PEDOT:PSS) is used as the hole injection layer, poly[(9,9-dioctylfluorenyl-2,7-diyl)-*co*-(4,49-(*N*-(4-*s*-butylphenyl))diphenylamine)] (TFB) as the hole transport layer, ZnCdSeS QD as the

DOI: 10.1021/acsphotonics.5b00267
ACS Photonics 2016, 3, 215−222

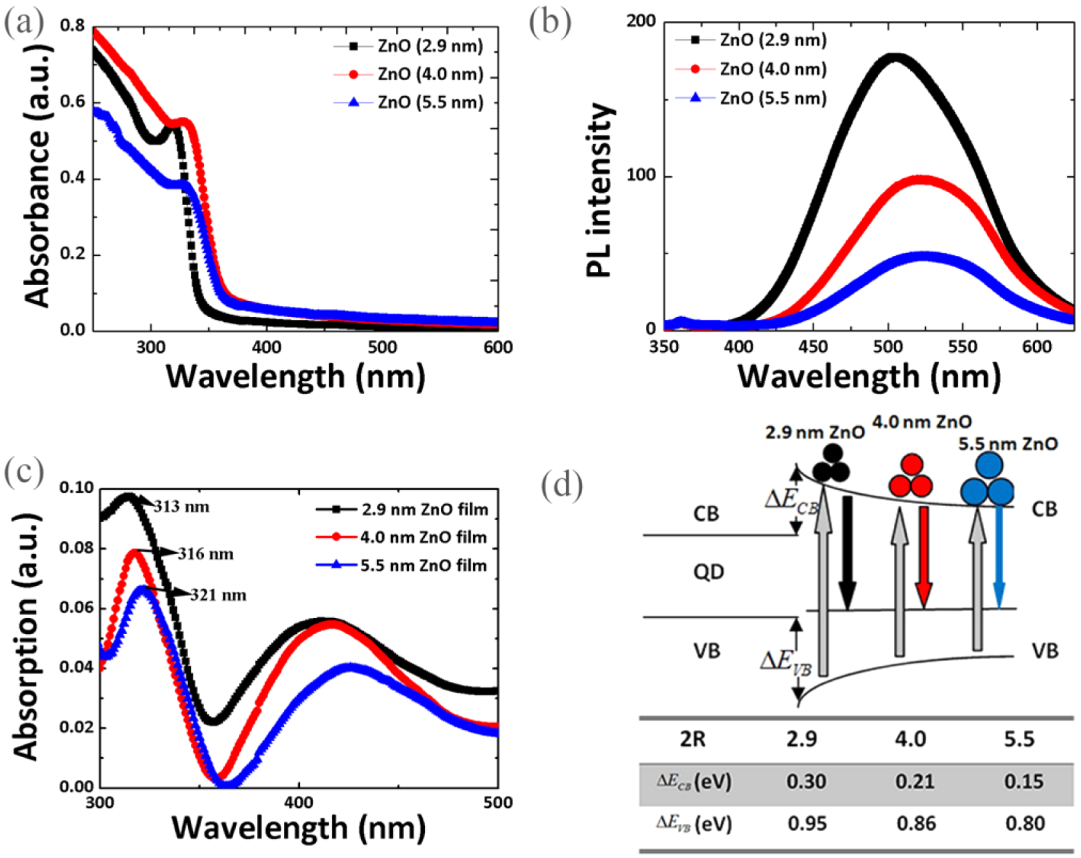

2R	2.9	4.0	5.5
ΔE_{CB} (eV)	0.30	0.21	0.15
ΔE_{VB} (eV)	0.95	0.86	0.80

Figure 4. (a) Absorption and (b) photoluminescence spectra of different size colloidal ZnO NPs. (c) Absorption spectra of ZnO film based on different size NPs and (d) corresponding band structure and table inset indicates band offsets at the QD and ZnO NPs layer interface.

emission layer, and ZnO NPs for electron injection, and transport. According to Figure 1b, the small conduction band offset and large valence band offset at the QD/ZnO nanoparticle interface stems from the ~3.8 eV electron affinity and ~7.4 eV ionization potential of ZnO NPs.[13,14] Thus, the ZnO NPs layer not only facilitates efficient electron injection from the Al cathode into QDs, but also prevents leakage of holes to the adjacent ZnO NPs layer. This confines the excitation-recombination region, thereby improving charge recombination efficiency.

Transmission electron microscopy (TEM) images of the three ZnO nanoparticle samples are shown in Figure 2. We found that the ratio $[Zn^{2+}]/[OH^-]$ of 1:0.5, 1:1, and 1:1.5, gave us average particle sizes of about 2.9, 4.0, and 5.5 nm, respectively. This illustrates that the concentration of $[OH^-]$ has a strong bearing on particle size. When the ratio of $[Zn^{2+}]/[OH^-]$ was 1:0.5, the concentration of $[Zn^{2+}]$ was higher than that of $[OH^-]$, leading to excess $[Zn^{2+}]$ left in the reacted solution, which limits the size of the ZnO NPs. As the concentration of $[OH^-]$ increased, the reaction rate is accelerated and the size of ZnO NPs is increased.[15] It is worth noting that when the ratio of $[Zn^{2+}]/[OH^-]$ is higher than 1:0.5, the sol−gel solution could hardly be formed, thus, making it difficult to produce ZnO NPs. On the other hand, if the ratio of $[OH^-]/[Zn^{2+}]$ exceeds 1.5:1, the ZnO NPs are severely aggregated and bulk ZnO is formed. In addition, lattice fringes can be clearly observed in the high-resolution TEM image, which suggests good crystallinity of the ZnO NPs.

The morphologies of the ZnO films for the different sized ZnO NPs after deposition on the substrate were revealed by the HRTEM images shown as Figure 3. It is found that the ZnO film was crystalline, which is due to postannealing. Compared to the ZnO NPs dispersed in solution, the ZnO NPs size does not change any more after deposition. The size of the ZnO NPs in films can be calculated from ~2.9 to ~5.5 nm for the three samples.

In order to study the band gap and quantum effects of the different ZnO NPs, their absorption and photoluminescence spectra were measured as shown in Figure 4a and b, respectively. It is observed that the peak position of absorption was located at 320 nm for the 2.9 nm NPs. This corresponds to the largest band gap among the three samples. The band gap E_g of the colloidal ZnO NPs is determined from the intercept between the wavelength axis and the tangent to the linear section of the absorption band edge.[15] The band gap is 3.65 eV for the 2.9 nm NPs. The energy band gap for the 4.0 and 5.5 nm ZnO NPs was retrieved as 3.47 and 3.35 eV, respectively. These values are higher than that of bulk ZnO (3.2−3.3 eV),[16] indicating that there is higher spatial confinement of photogenerated charge carriers in the smaller ZnO particles.[13,17] It is found that the tendency of band gap enlargement with decreasing size is consistent with the relation based on effective mass approximation (Figure S1, Supporting Information).[18]

$$E_{(\mathrm{gap,dot})} = E_{(\mathrm{gap,bulk})} + \frac{h^2}{8R^2}\left(\frac{1}{m_e^*} + \frac{1}{m_h^*}\right) - 0.248E_{\mathrm{Ryd}}^*$$

Here $E_{(\mathrm{gap,dot})}$ and $E_{(\mathrm{gap,bulk})}$ are the band gaps of ZnO NPs and bulk ZnO, respectively, E_{Ryd}^*, R and h the bulk exciton binding energy (60 meV), the particles' radius, and Planck's constant,

DOI: 10.1021/acsphotonics.5b00267
ACS Photonics 2016, 3, 215−222

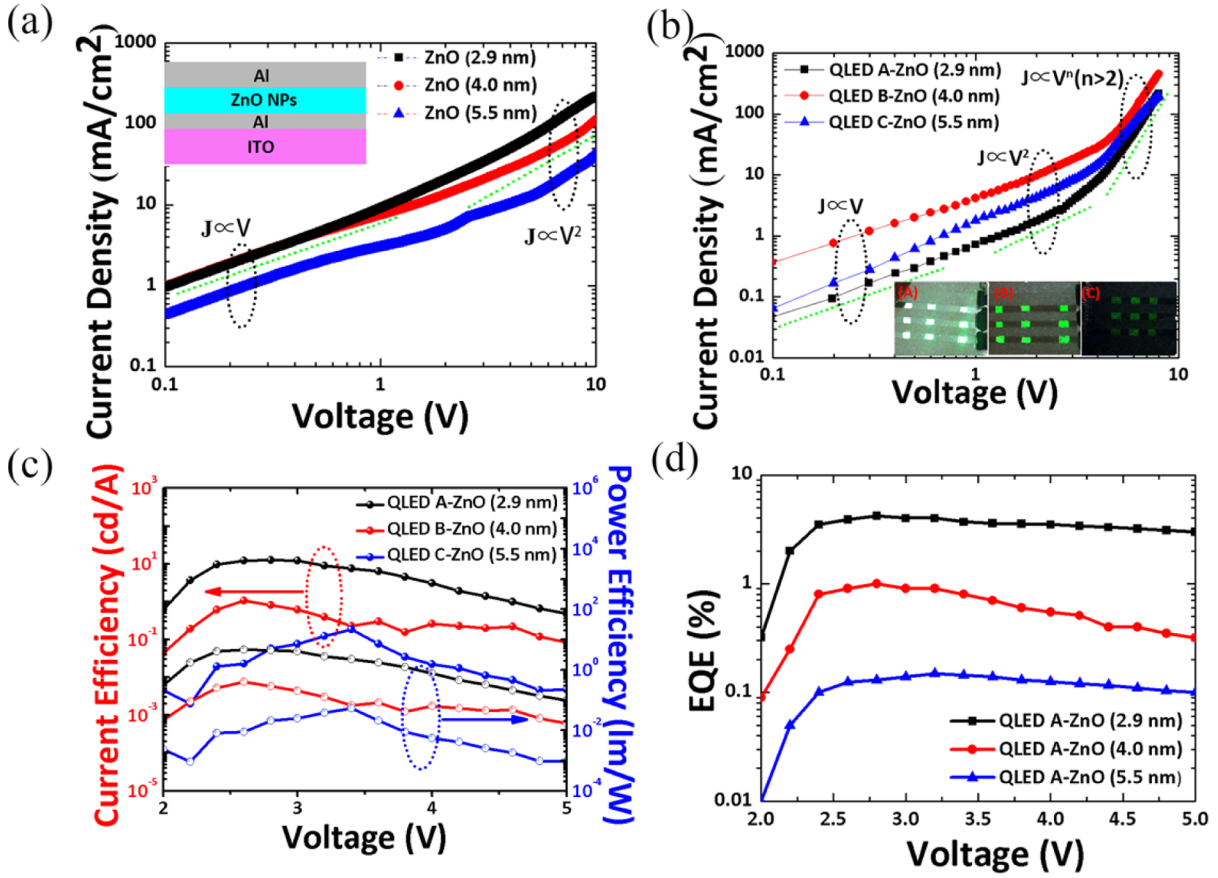

Figure 5. (a) Current density−voltage (J−V) characteristics of an electron-only device (ITO/Al/ZnO/Al) (inset shows structure of the electron-only device), (b) current-density voltage (J−V) characteristics of ZnO nanoparticle-based QLEDs. Three different regimes of conduction are clearly visible (inset shows luminance photos of QLED A, QLED B, and QLED C from left to right, respectively), (c) current and power efficiency characteristics for ZnO NPs-based QLEDs, and (d) EQE as a function of voltage for ZnO NPs-based QLEDs.

respectively. The effective masses $m_e^* = 0.24\ m_o$ and $m_h^* = 0.59\ m_o$ correspond to that of the electron and hole, respectively. From Figure 4b, we observe two peaks in the PL spectra. The intensity of one peak is relatively weak and located at the fundamental absorption band edge of the NP. This can be attributed to the direct electron−hole recombination.[19] The other peak is much more intense and is located at 500−550 nm, reflecting radiative recombination of electrons and holes, involving traps or structural defects on the surface of the NPs.[20] Figure 4c shows the absorption spectra of ZnO films formed by the different sized ZnO NPs. The UV−vis absorption peaks differ with each other, indicating that the ZnO NPs maintained the same size after annealing. From Figure 4b, it can be seen that the peak photoluminescence was red-shifted as the size of the NPs is increased due to recombination of charge at the conduction band-edge and deep trap levels.[21] This is explained by the schematic diagram in Figure 4d, which captures the effect of size on band structure and the corresponding energy band (indicated in the inset). As the size of the ZnO NPs increases from 2.9 to 5.5 nm, the conduction band-edge correspondingly drops from −3.80 to −3.95 eV and the valence band-edge rises from −7.45 to −7.30 eV. This is because of the weaker quantum confinement as deduced from ultraviolet photoelectron spectroscopy (UPS) measurements (Figure S2, Supporting Information). Here the deep trap level is assumed to remain the same.[22] The values of the conduction (E_{CB}) and valence (E_{VB}) bands retrieved from the UPS measurements corroborate with theoretically calculated values.[23] Because of the change in the ZnO NPs size, the conduction and valence band offsets at the QD and ZnO NPs layer interface decreases, as shown in the inset of Figure 4d. This has a strong bearing on device performance as discussed in the next section.

In order to investigate the effect of ZnO NPs size on the performance of QLEDs, the current-density voltage (J−V) characteristics of an electron only device with a structure of ITO/Al/ZnO NPs/Al and ZnO NPs-based QLEDs are displayed in Figure 5a and b, respectively. The J−V curve in Figure 5a clearly depicts two regions, the ohmic region (J∼V) below 1 V and space charge limited current (SCLC) region (J∼V^2) at higher operating voltages.[24] The J−V slope of the QLEDs in Figure 5b has unity gradient between 0.1 and 1 V depicting an ohmic region. The increase in the J−V slope up to 2 is representative of space charge limited conduction and further increase in the slope (at about 4 V) coincides with the onset of electroluminescence, that is, onset of both electron and hole injection into the QDs.[25] There is similar trend observed for variation in the J−V characteristics both in the electron only device and the QLED, because the J−V characteristics in both device consist of the ohmic region (J∼V) below 1 V and space charge limited current (SCLC) region (J∼V^2) at higher operating voltages. This phenomenon indicates the conductivity of ZnO has a great effect on the QLED performance. In addition, from Figure 5a, it can be seen that the conductivity of ZnO NPs film increases with the decrease in the ZnO NPs size. This is in accordance with the effective electron mobility in the

DOI: 10.1021/acsphotonics.5b00267
ACS Photonics 2016, 3, 215−222

NP sizes, which are 4.8×10^{-3}, 2.6×10^{-3}, and 7.2×10^{-4} $cm^2/V{\cdot}s$ for 2.9, 4.0, and 5.5 nm ZnO NPs, respectively (see Figure S3, Supporting Information). The decrease of the size of ZnO NPs leads to an increase in grain boundaries effect, leading to enhancing conductivity, which is similar to the condition in other metal oxide NPs.[26] All devices in Figure 5b exhibit a low turn-on voltage of 3.3 V (QLED A), 3.8 V (QLED B), and 4.3 V (QLED C). It can be seen that the smaller ZnO NPs lead to lower turn-on voltage resulting into higher power efficiency and better device stability (see Figure S4, Supporting Information). The inset of Figure 5b shows photos of QLED A−C under an applied voltage of 5 V. We see that QLED A presents the best performance with the highest luminance intensity.

The EL spectra for sample A are presented in Figure S5. We see that the position of the EL peak is located at 545 nm. The peak wavelength is red-shifted from the photoluminescence (PL) of the QD solution (Figure S6, Supporting Information), stemming from a combination of finite dot-to-dot interactions in close-packed solid films and the electric-field-induced Stark effect.[27] Its intensity increases with increasing applied voltage. The QLED performance from the standpoint of current and power efficiencies, as shown in Figure 5c, can be largely improved by decreasing the size of the NPs. The maximum current efficiency increased from 0.184 to 12.5 cd/A and the maximum power efficiency increased from 0.054 to 4.69 lm/W as the size of the ZnO NPs decreased from 5.5 to 2.9 nm. More importantly, the external quantum efficiencies (EQE) of device can be largely improved from 0.15% to 4.2% as the size of the ZnO NPs decreased from 5.5 to 2.9 nm, as displayed in Figure 5d. In addition, the reproducibility of the results from device to device is very good (Figure S7, Supporting Information). Moreover, the device performance in our paper is very similar to that in previously published papers, which testifies to the reliability and accuracy of our experiment results and the consistency of our experimental results. (Tables S3 and S4, Supporting Information)

The variation of the performance of QLED based on different size of ZnO NPs can be attributed to the change in energy band of ZnO NPs because of quantum confinement. In other words, the smaller ZnO NPs improving QLED performance is due to the more favorable energy bands of the ZnO NPs which serve to enhance electron transport because of quantum confinement. This is deduced by photoluminescence and absorption spectra, and UPS measurement of ZnO NPs. The favorable energy band for the smallest ZnO NPs is shown as follows: (i) Enhanced driving force for electron injection. As the size of ZnO NPs decreases, the conduction band-edge ascends and the valence band-edge descends because of the stronger quantum confinement effect. Thus, the shifted conduction band level of ZnO NPs as shown in the Figure 4d leads to favorable electron transfer from the ZnO ETL to the QD layer because of a stronger driving force.[28] (ii) Benefit for hole blocking. The energy offset between the valence bands of the QD and ZnO NPs becomes larger. This results in better blockage of holes from the QDs to adjacent the ZnO NP layer thus increasing the charge recombination efficiency. (iii) Enhanced Auger assisted charge injection. The Auger-assisted charge injection occurring at the QD/TFB interface strongly depends on the level of electron injection into the QD layer.[29] Therefore, QLEDs with smaller size NPs as the ETL require lower voltages to accumulate sufficient electron concentration for an efficient Auger process because of its favorable band structure for electron injection. This decreases the turn on voltage and increases the power efficiency of QLEDs. (iv) The device stability is strongly dependent on the balance of carrier injection. Moreover, the balance of carrier injection is related to the band structure of ZnO NPs. Thus, the device stability is directly involved with the band structure of ZnO NPs. As can be seen in Figure 4d, smaller energy barrier with corresponding injection force are typically associated with larger size NPs, which leads to the imbalanced carrier injection. Consequently, the imbalanced carrier (electron or hole) injection into the QD layer can give rise to nonradiative recombination, which leads to device heating and thus instability. The same phenomenon was also observed in earlier reports.[28] As expected, the smaller ZnO NPs show better stability because of the balanced carriers injection due to favorable band offsets, hence increase radiative recombination and so the stability.[9]

In order to study the size effect of ZnO NPs on the exciton dissociation in the adjacent QD layer, devices with ITO/QD/ZnO structure were fabricated. The exciton dissociation is caused by the emission quenching of QDs.[10] Similar to other metal oxides, the ZnO quenches the quantum yield of QDs by virtue of an ultrafast nonradiative process.[30] The PL decay dynamics of the QDs based on the different size of ZnO NPs with excitation wavelength of 375 nm are shown in Figure 6.

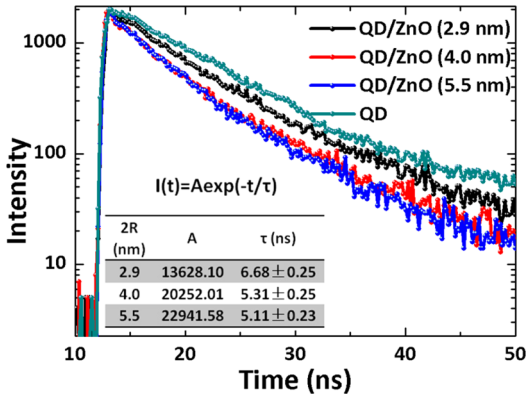

Figure 6. Time-resolved PL dynamics of QD film on ITO and QD film on ITO/QD/ZnO structure. Inset shows corresponding parameters for one-exponential fitting for time-resolved fluorescence dynamics.

The decay lifetime of original QDs is calculated as 8.12 (error bar is ±0.28) ns, which is larger than that of QDs with ZnO NPs film. The result is comparable to that in a previous paper,[31] which indicates that the QD has a longer decay lifetime deposited on glass compared to that deposited on metal oxide. In addition, the QDs exhibit significantly increased PL lifetime with decreasing size of ZnO NPs. The PL lifetime decay curves of QDs with different size of ZnO NPs can be well fitted by a one-exponential function defined as $I(t) = A \exp(-t/\tau)$.[32] The one-exponential fit shows the highest fidelity among the series of exponential fits. The average decay time τ are 6.68, 5.31, and 5.11 ns, for 2.9, 4.0, and 5.5 nm ZnO NPs, respectively. According to a series of experiments (Figure S8, Supporting Information), it is found that the charge separation can be considered as one of the major origins of the lifetime changes; Meanwhile, other processes may also contribute to the change of decay lifetime more or less, such as the photochemical reaction on the QD surface, change on the QD surface due to chemicals remaining on the ZnO NP layer, QD layer formation

DOI: 10.1021/acsphotonics.5b00267
ACS Photonics 2016, 3, 215−222

(FRET transfer), and changes in surrounding permittivity. The decay lifetime is seen to increase monotonically as the size of ZnO NPs is decreased due to the larger energy offset at the QD/ZnO interface. For the smaller sized ZnO NPs, the conduction band-edge ascends to a greater degree so that the energy difference between the conduction band levels of the QD and ZnO NP layer is larger, as displayed in Figure 4d. Hence, fewer excitons are dissociated and electron transfer from QDs to ZnO NPs is weaker, causing decreased fluorescence quenching.[33] The exciton dissociation in QDs by charge transfer to adjacent electron transport layer can decrease the PL quantum efficiency of the QDs, leading to low quantum efficiency of QLEDs.[34]

CONCLUSIONS

In this paper we demonstrated the size tunability of sol−gel synthesized ZnO nanoparticles in the electron transport layer in quantum dot LEDs (QLEDs) and, in particular, examined its impact on electron injection and hole quantum confinement. Measurements of photoluminescence decay lifetime and electron mobility show that decreasing the nanoparticle size results in significant increase in the electron decay lifetime and electron transport, all of which serve to lower the turn-on voltage and improve the power efficiency. A comparison of nanoparticle sizes shows that the best performance is achieved with the smallest size (~2.9 nm). This yields band offsets that are favorable for electron transfer and equally conducive to hole confinement in the adjacent quantum dot layer, thereby boosting the charge recombination efficiency of the QLED. While the QLED performance reported here can benefit from further device optimization, the results pave the way for use of other metal oxide nanoparticles in charge transport layers in QLEDs.

ASSOCIATED CONTENT

Supporting Information

The Supporting Information is available free of charge on the ACS Publications website at DOI: 10.1021/acsphotonics.5b00267.

Relationship between size and bandgap, UPS spectrum of ZnO film, the mobility characterization of ZnO films, stability of device, characterization of QDs, and reproducible test (PDF).

AUTHOR INFORMATION

Corresponding Authors

*E-mail: lw@seu.edu.cn.

*Phone: +86 25 83792449. Fax: +86 25 833632222. E-mail: an299@cam.ac.uk.

Author Contributions

‡These authors contributed equally (J.P. and J.C.).

Notes

The authors declare no competing financial interest.

ACKNOWLEDGMENTS

This work was supported partially by the National Key Basic Research Program 973 (2013CB328804, 2013CB328803), the National High-Tech R&D Program 863 of China (2012AA03A302, 2013AA011004), National Natural Science Foundation Project (51120125001, 61271053, 61306140, 61405033, 91333118, 61372030, 61307077, and 51202028), Beijing Natural Science Foundation (4144076), and Natural Science Foundation Project of Jiangsu Province (BK20141390, BK20130629, BK20151417 and BK20130618).

REFERENCES

(1) Coe, S.; Woo, W. K.; Bawendi, M.; Bulovic, V. Electroluminescence from Single Monolayers of Nanocrystals in Molecular Organic Devices. *Nature* **2002**, *420*, 800−803.

(2) Coe-Sullivan, S.; Steckel, J. S.; Woo, W. K.; Bawendi, M. G.; Bulovic, V. Large-area Ordered Quantum-dot Monolayers via Phase Separation During Spin-casting. *Adv. Funct. Mater.* **2005**, *15*, 1117−1124.

(3) Colvin, V. L.; Schlamp, M. C.; Alivisatos, A. P. Light-emitting Diodes Made From Cadmium Selenide Nanocrystals and a Semiconducting Polymer. *Nature* **1994**, *370*, 354−357.

(4) Mueller, A. H.; Petruska, M. A.; Achermann, M.; Werder, D. J.; Akhadov, E. A.; Koleske, D. D.; Hoffbauer, M. A.; Klimov, V. I. Multicolor Light-emitting Diodes Based on Semiconductor Nanocrystals Encapsulated in GaN Charge Injection Layers. *Nano Lett.* **2005**, *5*, 1039−1044.

(5) Caruge, J. M.; Halpert, J. E.; Wood, V.; Bulovic, V.; Bawendi, M. G. Colloidal Quantum-dot Light-emitting Diodes with Metal-oxide Charge Transport Layers. *Nat. Photonics* **2008**, *2*, 247−250.

(6) Cho, K.-S.; Lee, E. K.; Joo, W.-J.; Jang, E.; Kim, T.-H.; Lee, S. J.; Kwon, S.-J.; Han, J. Y.; Kim, B.-K.; Choi, B. L.; Kim, J. M. High-performance Crosslinked Colloidal Quantum-dot Light-emitting Diodes. *Nat. Photonics* **2009**, *3*, 341−345.

(7) Feng, X. J.; Shankar, K.; Varghese, O. K.; Paulose, M.; Latempa, T. J.; Grimes, C. A. Vertically Aligned Single Crystal TiO_2 Nanowire Arrays Grown Directly on Transparent Conducting Oxide Coated Glass: Synthesis Details and Applications. *Nano Lett.* **2008**, *8*, 3781−3786.

(8) Lee, K. H.; Lee, J. H.; Song, W. S.; Ko, H.; Lee, C.; Lee, J. H.; Yang, H. Highly Efficient, Color-pure, Color-stable Blue Quantum Dot Light-emitting Devices. *ACS Nano* **2013**, *7*, 7295−7302.

(9) Qian, L.; Zheng, Y.; Xue, J. G.; Holloway, P. H. Stable and Efficient Quantum-dot Light-emitting Diodes Based on Solution-processed Multilayer Structures. *Nat. Photonics* **2011**, *5*, 543−548.

(10) Mashford, B. S.; Stevenson, M.; Popovic, Z.; Hamilton, C.; Zhou, Z. Q.; Breen, C.; Steckel, J.; Bulovic, V.; Bawendi, M.; Coe-Sullivan, S.; Kazlas, P. T. High-efficiency Quantum-dot Lght-emitting Devices with Enhanced Charge Injection. *Nat. Photonics* **2013**, *7*, 407−412.

(11) Shirasaki, Y.; Supran, G. J.; Bawendi, M. G.; Bulović, V. Emergence of Colloidal Quantum-dot Light-emitting Technologies. *Nat. Photonics* **2012**, *7*, 13−23.

(12) Chen, J.; Lei, W.; Li, Z.; Pan, J.; Li, Q.; Xia, J.; Tu, Y. P-87: All Solution Processable of Color Tunable Quantum Dot Light-Emitting Diodes; *SID Symposium Dig. Tech. Pap.*; SID, 2014; pp 1312−1314.

(13) Bahnemann, D. W.; Kormann, C.; Hoffmann, M. R. Preparation and Characterization of Quantum Size Zinc Oxide: A Detailed Spectroscopic Study. *J. Phys. Chem.* **1987**, *91*, 3789−3798.

(14) van Dijken, A.; Meulenkamp, E. A.; Vanmaekelbergh, D.; Meijerink, A. Identification of the Transition Responsible for the Visible Emission in ZnO Using Quantum Size Effects. *J. Lumin.* **2000**, *90*, 123−128.

(15) Panasiuk, Y. V.; Raevskaya, O. E.; Stroyuk, O. L.; Kuchmiy, S. Y.; Dzhagan, V. M.; Hietschold, M.; Zahn, D. R. T. Colloidal ZnO Nanocrystals in Dimethylsulfoxide: a New Synthesis, Optical, Photo- and Electroluminescent Properties. *Nanotechnology* **2014**, *25*, 075601.

(16) Ozgur, U.; Alivov, Y. I.; Liu, C.; Teke, A.; Reshchikov, M. A.; Dogan, S.; Avrutin, V.; Cho, S. J.; Morkoc, H. A Comprehensive Review of ZnO Materials and Devices. *J. Appl. Phys.* **2005**, *98*, 041301.

(17) Kamat, P. V.; Patrick, B. Photophysics and Photochemistry of Quantized Zinc Oxide Colloids. *J. Phys. Chem.* **1992**, *96*, 6829−6834.

(18) Fu, Y. S.; Du, X. W.; Kulinich, S. A.; Qiu, J. S.; Qin, W. J.; Li, R.; Sun, J.; Liu, J. Stable Aqueous Dispersion of ZnO Quantum Dots with

DOI: 10.1021/acsphotonics.5b00267
ACS Photonics 2016, 3, 215−222

Strong Blue Emission via Simple Solution Route. *J. Am. Chem. Soc.* **2007**, *129*, 16029−16033.
(19) Stroyuk, O. L.; Dzhagan, V. M.; Shvalagin, V. V.; Kuchmiy, S. Y. Size-Dependent Optical Properties of Colloidal ZnO Nanoparticles Charged by Photoexcitation. *J. Phys. Chem. C* **2010**, *114*, 220−225.
(20) Spanhel, L.; Anderson, M. A. Semiconductor Clusters in the Sol-gel Process: Quantized Aggregation, Gelation, and Crystal Growth in Concentrated Zinc Oxide Colloids. *J. Am. Chem. Soc.* **1991**, *113*, 2826−2833.
(21) Zhang, L. Y.; Yin, L. W.; Wang, C. X.; Lun, N.; Qi, Y. X.; Xiang, D. Origin of Visible Photoluminescence of ZnO Quantum Dots: Defect-Dependent and Size-Dependent. *J. Phys. Chem. C* **2010**, *114*, 9651−9658.
(22) Gu, Y.; Kuskovsky, I. L.; Yin, M.; O'Brien, S.; Neumark, G. F. Quantum Confinement in ZnO Nanorods. *Appl. Phys. Lett.* **2004**, *85*, 3833−3835.
(23) Stroyuk, A.; Shvalagin, V.; Kuchmii, S. Y. Photochemical Synthesis and Optical Properties of Binary and Ternary Metal-semiconductor Composites Based onZinc Oxide Nanoparticles. *J. Photochem. Photobiol., A* **2005**, *173*, 185−194.
(24) Dai, X.; Zhang, Z.; Jin, Y.; Niu, Y.; Cao, H.; Liang, X.; Chen, L.; Wang, J.; Peng, X. Solution-processed, High-performance Light-emitting Diodes Based on Quantum Dots. *Nature* **2014**, *515*, 96−99.
(25) Hikmet, R.; Talapin, D.; Weller, H. Study of Conduction Mechanism and Electroluminescence in CdSe/ZnS Quantum Dot Composites. *J. Appl. Phys.* **2003**, *93*, 3509−3514.
(26) Biju, V.; Khadar, M. A. DC Conductivity of Consolidated Nanoparticles of NiO. *Mater. Res. Bull.* **2001**, *36*, 21−33.
(27) Xu, W.; Ji, W. Y.; Jing, P. T.; Yuan, X.; Wang, Y. A.; Xiang, W. D.; Zhao, J. L. Efficient Inverted Quantum-dot Light-emitting Devices with TiO2/ZnO Bilayer as the Electron Contact Layer. *Opt. Lett.* **2014**, *39*, 426−429.
(28) Robel, I.; Kuno, M.; Kamat, P. V. Size-Dependent Electron Injection from Excited CdSe Quantum Dots into TiO_2 Nanoparticles. *J. Am. Chem. Soc.* **2007**, *129*, 4136−4137.
(29) Qian, L.; Zheng, Y.; Choudhury, K. R.; Bera, D.; So, F.; Xue, J. G.; Holloway, P. H. Electroluminescence from Light-emitting Polymer/ZnO Nanoparticle Heterojunctions at Sub-bandgap Voltages. *Nano Today* **2010**, *5*, 384−389.
(30) Yang, X. Y.; Mutlugun, E.; Dang, C.; Dev, K.; Gao, Y.; Tan, S. T.; Sun, X. W.; Demir, H. V. Highly Flexible, Electrically Driven, Top-Emitting, Quantum Dot Light-Emitting Stickers. *ACS Nano* **2014**, *8*, 8224−8231.
(31) Wu, X. Y.; Yeow, E. K. L. Charge-transfer Processes in Single CdSe/ZnS Quantum Dots with P-type NiO Nanoparticles. *Chem. Commun.* **2010**, *46*, 4390−4392.
(32) Morello, G.; Anni, M.; Cozzoli, P. D.; Manna, L.; Cingolani, R.; De Giorgi, M. Picosecond Photoluminescence Decay Time in Colloidal Nanocrystals: The Role of Intrinsic and Surface States. *J. Phys. Chem. C* **2007**, *111*, 10541−10545.
(33) Jin, S. Y.; Lian, T. Q. Electron Transfer Dynamics from Single CdSe/ZnS Quantum Dots to TiO_2 Nanoparticles. *Nano Lett.* **2009**, *9*, 2448−2454.
(34) Zhang, Y. L.; Jing, P. T.; Zeng, Q. H.; Sun, Y. J.; Su, H. P.; Wang, Y. A.; Kong, X. G.; Zhao, J. L.; Zhang, H. Photoluminescence Quenching of CdSe Core/Shell Quantum Dots by Hole Transporting Materials. *J. Phys. Chem. C* **2009**, *113*, 1886−1890.

DOI: 10.1021/acsphotonics.5b00267
ACS Photonics 2016, 3, 215−222